*Annals of Biomedical Engineering*, Vol. 21, pp. 591–603, 1993
Printed in the USA. 

0090-6964/93 $6.00 + .00


# Nonlinear Analysis of Renal Autoregulation Under Broadband Forcing Conditions

VASILIS Z. MARMARELIS,*† KI H. CHON,* YU-MING CHEN,‡
DONALD J. MARSH,*‡ and N.-H. HOLSTEIN-RATHLOU‡

*Department of Biomedical Engineering, †Department of Electrical Engineering,
‡Department of Physiology and Biophysics, University of Southern California, Los Angeles, CA

**Abstract**—Linear analysis of renal blood flow fluctuations, induced experimentally in rats by broad-band (pseudorandom) arterial blood pressure forcing at various power levels, has been unable to explain fully the dynamics of renal autoregulation at low frequencies (1). This observation has suggested the possibility of nonlinear mechanisms subserving renal autoregulation at frequencies below 0.2 Hz. This paper presents results of 3rd-order Volterra-Wiener analysis that appear to explain adequately the nonlinearities in the pressure-flow relation below 0.2 Hz in rats. The contribution of the 3rd-order kernel in describing the dynamic pressure-flow relation is found to be important. Furthermore, the dependence of 1st-order kernel waveforms on the power level of broadband pressure forcing indicates the presence of nonlinear feedback (of sigmoid type) based on previously reported analysis of a class of nonlinear feedback systems (11).

**Keywords**—Renal autoregulation, Nonlinear modeling, Wiener kernels.

## INTRODUCTION

Renal blood flow autoregulation (i.e., the process by which vascular hemodynamic impedance is adjusted to minimize fluctuations in blood flow caused by fluctuations in blood pressure) is critical for maintaining fairly constant filtration rates by the kidneys (3,13). Two important mechanisms subserving renal autoregulation are the myogenic and the tubuloglomerular feedback (TGF). The myogenic mechanism is vascular in nature and causes changes in blood vessel diameter and mechanical characteristics (e.g., stiffness) in response to changes in local vascular pressures. The TGF mechanism is governed by flow-rate dependent concentration changes in tubular fluid, sensed at the macula densa, and alters the impedance characteristics of the preglomerular vessels through still unknown mechanisms (17).

The frequency response characteristics of the two mechanisms have been studied in rats (1,4,15), and the general conclusion is that the myogenic mechanism causes a resonance (decreased impedance) over the frequency range from 0.1–0.2 Hz, while the TGF mechanism is active in the frequency range below 0.06–0.08 Hz where increased impedance is observed. The combined action of the two mechanisms attenuates the effect of blood pressure fluctuations on blood flow at frequencies less than 0.1 Hz, while the effect is accentuated in the 0.1–0.2 Hz frequency range.

Recent studies in rats have used broad-band arterial pressure fluctuations to separate the dynamical properties of the two renal autoregulatory mechanisms (2,4). The advantages of broadband forcing as an excitation in linear and nonlinear system identification have been well documented, and the associated modeling techniques have gained in popularity over the last 20 years (7,9,10). Suppression of noise and reduction of experimentation time are among these advantages. Another major advantage is the ability of this approach to discern quantitatively the linear and nonlinear dynamic characteristics of the system under study. This has been demonstrated in a number of applications, mostly in the area of neurophysiology. To explore the efficacy of this approach in renal autoregulation studies in rats and to extend the results of Holstein-Rathlou et al. (4), we have used broad-band arterial pressure forcings at various power levels. Our objective is to obtain nonlinear characterizations of the pressure-flow dynamic relation over the entire frequency range from 0 to 1 Hz within a broad dynamic range of blood pressure fluctuations. These nonlinear characterizations (in the form of Volterra-Wiener models) can be used to examine the nonlinear dynamics of renal autoregulation mechanisms. To this purpose, we employ a technique for Volterra-Wiener kernel estimation (12),

*Acknowledgments*—This work was supported by NIH grants No. RR-01861 (Biomedical Simulations Resource from the National Center of Research Resources) HL-45623 and DK-15968, and by a grant from the Whitaker Foundation.

Address correspondence to Vasilis Z. Marmarelis, Department of Biomedical Engineering, University of Southern California, Los Angeles, CA 90089.

*(Received 4/16/93)*

which allows accurate system identification to be extended to 3rd-order nonlinearities within the experimental constraints of this application.

The Experimental Procedures and Data Collection section describes the experimental preparation and data collection procedures. The Nonlinear Modeling Methodology section presents a summary of the data analysis and nonlinear modeling technique. The Results section presents the results, and the main conclusions are summarized in the Conclusions and Discussion section.

## EXPERIMENTAL PROCEDURES AND DATA COLLECTION

Experiments were performed on male Sprague-Dawley rats weighing 210–370 g. The animals had free access to food and tap water prior to experiments. Anesthesia was induced by placing each rat in a Plexiglas chamber containing 5% halothane administered in 25% oxygen and 75% nitrogen through a Fluotec Mark-3 vaporizer. A tracheostomy was performed and the rats were placed on a servo-controlled heated operating table which maintained their body temperature at 37°C.

The rats were connected to a small animal respirator (Harvard model 683) adjusted to maintain arterial blood pH between 7.35 and 7.45 with a mixture of 25% oxygen and 75% nitrogen. Tidal volume ranged from 1.9–2.5 ml, depending on body weight, with a frequency of 57–60 breaths per minute. The final concentration of halothane needed to maintain sufficient anesthesia was approximately 1%. A polyethylene catheter (PE 50) was placed in the right jugular vein for infusions. After a priming dose of 6 mg gallamine triethiodide (Flaxedil) in 1 ml 0.9% saline, a continuous intravenous infusion of 60 mg gallamine triethiodide in 10 ml 0.9% saline was given at 20 ml/min.

The abdomen was opened through a midline incision extended to the left flank. The distal aorta was dissected free and cannulated at the bifurcation with a Teflon tube filled with blood freshly obtained from a littermate. To avoid clot formation in the tube, Heparin was added to the blood in a concentration of 10 units/ml. The Teflon tube led to a glass tube where low viscosity silicone oil made an interface with the blood. A polyethylene tube, also filled with silicone oil, connected the glass tube to a stainless steel bellows 3 cm in diameter and 5 cm long. The bellows was filled with the low viscosity oil and connected to a linear motor (Ling Dynamic Systems Ltd., Royston, England) controlled by an IBM AT computer. The left kidney was placed in a Lucite cup and superfused with saline preheated to 37°C.

The left kidney was denervated by dissecting the renal artery, carefully stripping away all nerves and wiping the artery with a solution of 5% phenol dissolved in ethanol. The ureter was cannulated to ensure free flow of urine. Experiments were started after a recovery period of 1 hour during which a plasma infusion corresponding to 15 ml/kg body weight was given to replace surgical fluid losses. A constant infusion of plasma at a rate 1.5 ml/kgBW/h was given throughout the experiment.

Arterial pressure was measured in the superior mesenteric artery with a catheter (PE 90) filled with heparinized saline (10 U/ml) connected to a Statham-Gould P23dB pressure transducer. Renal blood flow was measured in the left renal artery with an electromagnetic flow probe (Carolina Medical Electronics, King, NC) connected to an electromagnetic blood flow meter (Biotronics Laboratory, model BL-610, Silver Spring, MD).

Measurements of renal blood flow and arterial blood pressure were made while broadband fluctuations were induced in the arterial blood pressure. These were generated by the bellows pump through the blood filled cannula inserted into the distal aorta at the bifurcation. The linear motor that moved the bellows was driven by a power amplifier (Hewlett-Packard, HP 6824A) controlled by an IBM AT computer through a digital-to-analog converter (Data Translation). The input to the D/A converter was derived from a constant-switching-pace symmetric random signal (CSRS) which exhibits the spectral properties of band-limited white noise (8). A unique seed was used for the random number generator in each experiment. The series of random numbers was supplied to the D/A converter at a frequency of 2 Hz. The maximum amplitude of the pump excursion is established by the voltage supplied to the pump from the power supply. Three different levels were used in each experiment to vary the power of the forcing. Four experiments on different preparations were performed at each level, yielding a total of 12 arterial pressure and 12 blood flow data records.

The rats were allowed to stabilize to the forcing for at least 2 minutes. After this period the renal blood flow and arterial pressure signals were recorded on a TEAC R-61 cassette data recorder for off-line analysis. When the data were replayed from the tape recorder, the signals were passed through a second order low-pass Butterworth anti-aliasing filter with the cutoff frequency set at 1.5 Hz, and were then sampled with a 12-bit analog-to-digital converter (Data Translation) connected to a microcomputer with an Intel 80286 CPU.

The three different levels of arterial pressure forcing used in each of the four preparations (as measured by the RMS value of the resulting pressure fluctuations) varied from experiment to experiment, and they formed three groups: low (3.86–5.66 mmHg), medium (6.33–7.96 mmHg), and high (10.40–12.41 mmHg) level, according to the RMS values of arterial pressure fluctuations shown in Table 1.

The experimental data used for analysis were obtained

**TABLE 1. Mean and Root-Mean-Square (RMS) values of arterial pressure (AP) and renal blood flow (BF) for 3 different power level forcings and four experimental preparations (rats).**

| Data Set No. (Exp. Prep.) | Power Level | AP Mean, mmHg | AP RMS, mmHg | BF Mean, ml/min | BF RMS ml/min |
|---|---|---|---|---|---|
| 1 | High | 94.19 | 10.40 | 5.72 | 0.83 |
| | Medium | 109.13 | 6.33 | 6.24 | 0.50 |
| | Low | 105.69 | 3.99 | 6.42 | 0.33 |
| 2 | High | 88.96 | 11.58 | 3.97 | 1.06 |
| | Medium | 99.21 | 6.92 | 4.12 | 0.65 |
| | Low | 102.38 | 3.86 | 4.54 | 0.39 |
| 3 | High | 92.26 | 12.41 | 4.15 | 0.88 |
| | Medium | 96.41 | 7.69 | 4.81 | 0.56 |
| | Low | 105.32 | 5.28 | 5.71 | 0.37 |
| 4 | High | 112.29 | 11.64 | 10.62 | 1.26 |
| | Medium | 115.08 | 7.96 | 10.11 | 0.82 |
| | Low | 118.54 | 5.66 | 9.24 | 0.71 |

Note that the mean values generally decrease with increasing power level.

over 256 seconds with a sampling rate of 2 samples per second (Nyquist frequency of 1 Hz), after digital low-pass filtering (using a 20th order Hamming window) to avoid aliasing. Experimental data from 2 medium and 2 low forcing levels of arterial pressure and corresponding blood flow data records were subjected to 2nd-order polynomial trend removal. Each data-record containing 512 data-points was de-meaned (by subtracting out the mean value) and normalized by dividing with the RMS value of each data-record. Thus, regardless of different arterial pressure forcings, all analyzed data sets had zero mean and unit variance.

## NONLINEAR MODELING METHODOLOGY

The experimental data were analyzed in the context of the Volterra-Wiener approach to nonlinear system identification (7). A 3rd-order Volterra model was considered as the nonlinear dynamic relation between the system input $x(t)$ (arterial blood pressure) and the system output $y(t)$ (renal blood flow):

$$y(t) = k_0 + \int_0^\infty k_1(\tau)x(t-\tau)\,d\tau + \int_0^\infty\int k_2(\tau_1,\tau_2)x(t-\tau_1)x(t-\tau_2)\,d\tau_1\,d\tau_2 + \int_0^\infty\int\int k_3(\tau_1,\tau_2,\tau_3)x(t-\tau_1)x(t-\tau_2) \times x(t-\tau_3)\,d\tau_1\,d\tau_2\,d\tau_3 \quad (1)$$

where the Volterra kernels $\{k_0, k_1, k_2, k_3\}$ characterize the dynamic properties of the system. The zeroth-order kernel is simply a constant offset value, and the 1st-order kernel $k_1(\tau)$ represents the linear component of the system dynamics. The 2nd-order kernel $k_2(\tau_1,\tau_2)$ and 3rd-order kernel $k_3(\tau_1,\tau_2,\tau_3)$ represent quadratic and cubic (nonlinear) system dynamics, respectively.

When the input $x(t)$ is Gaussian white-noise (GWN), the functionals of Eq. 1 can be orthogonalized to yield the corresponding Wiener model of 3rd-order (19):

$$y(t) = h_0 + \int_0^\infty h_1(\tau)x(t-\tau)\,d\tau + \left\{\int_0^\infty\int h_2(\tau_1,\tau_2)x(t-\tau_1)x(t-\tau_2)\,d\tau_1\,d\tau_2 - P\int_0^\infty h_2(\tau,\tau)\,d\tau\right\} + \left\{\int_0^\infty\int\int h_3(\tau_1,\tau_2,\tau_3)x(t-\tau_1)x(t-\tau_2) \times x(t-\tau_3)\,d\tau_1\,d\tau_2\,d\tau_3 - 3P\int_0^\infty\int h_3(\tau,\lambda,\lambda)x(t-\tau)\,d\tau\,d\lambda\right\} \quad (2)$$

where $P$ is the power level of the GWN input. The Wiener kernels are, in general, distinct from the Volterra kernels of a system, although both sets yield equivalent input-output models (if complete). Wiener introduced his orthogonalized series in order to provide a practical way of estimating individual kernels from actual input-output data. For details of this approach and recent developments in this area, the reader is referred to a number of books and monographs on the subject (7–10,14,16,19).

For the 3rd-order models of Eqs. 1 and 2, the relations among the Volterra and Wiener kernels are:

$$k_0 = h_0 - P\int_0^\infty h_2(\tau,\tau)\,d\tau \quad (3a)$$

$$k_1 = h_1(\tau) - 3P\int_0^\infty h_3(\tau,\lambda,\lambda)\,d\lambda \quad (3b)$$

$$k_2(\tau_1,\tau_2) = h_2(\tau_1,\tau_2) \quad (3c)$$

$$k_3(\tau_1,\tau_2,\tau_3) = h_3(\tau_1,\tau_2,\tau_3)\,. \quad (3d)$$

Since the true order of the system under study is usually unknown, practical estimation of kernels is based on the orthogonalized functional hierarchy suggested by Wie-

ner. Orthogonalization schemes have been developed for input ensembles other than GWN, e.g., multilevel pseudorandom inputs, Poisson spike-train inputs, etc. (for partial review see [7]). The most commonly used technique for kernel estimation has been the cross-correlation technique proposed by Lee and Schetzen in 1965 (6). Many investigators have proposed alternative kernel estimation techniques through the years, which are applicable under different sets of conditions and exhibit distinct blends of advantages and disadvantages. The cross-correlation technique, although popular, is far from being an optimum choice. Its main drawback is that it requires strict whiteness of the input and long data-records in order to yield kernel estimates of satisfactory accuracy. Among the many attempts to relax these requirements and improve estimation accuracy, Korenberg's exact orthogonalization technique (first proposed in 1987) is notable (5). A technique that employs Laguerre expansions of the system kernels was originally proposed by Wiener (19) and was first implemented by Watanabe and Stark (18). An improved implementation of this technique has been proposed recently by Marmarelis (12) and has been shown to exhibit significant advantages in certain cases where: (a) the input may deviate from whiteness; (b) the experimental data-records are relatively short; and (c) the system memory extent is long relative to the system bandwidth (i.e., the kernels need to be estimated over many time lags). Such a situation is found in this application to renal autoregulation data: the pressure forcing input inevitably deviates from whiteness due to uncontrollable experimental reasons; the experimental data-records can not be too long due to preparation instabilities; the system memory is long relative to the system bandwidth (which dictates that at least 60 lags be computed along each kernel dimension). Furthermore, this technique allows compact representation of the kernels (due to the Laguerre expansion) making possible the practical estimation of accurate 3rd-order kernels from short experimental data-records.

This technique employs the orthonormal set of Laguerre functions $\{L_j(t)\}$ to expand the system kernels, e.g.,

$$k_n(\tau_1,\ldots,\tau_n) = \sum_{j_1}\cdots\sum_{j_n} c_n(j_1,\ldots,j_n)L_{j_1}(\tau_1)\ldots L_{j_n}(\tau_n) \quad (4)$$

where $\{c_n(j_1,\ldots j_n)\}$ are the (unknown) expansion coefficients. Then the Volterra model of Eq. 1 becomes:

$$y(t) = k_0 + \sum_j c_1(j)v_j(t) + \sum_{j_1}\sum_{j_2} c_2(j_1,j_2)v_{j_1}(t)v_{j_2}(t) + \sum_{j_1}\sum_{j_2}\sum_{j_3} c_3(j_1,j_2,j_3)v_{j_1}(t)v_{j_2}(t)v_{j_3}(t) \quad (5)$$

where

$$v_j(t) = \int_0^{\mu} L_j(\tau)x(t-\tau)\,d\tau \quad (6)$$

and $\mu$ is the extent of the system memory (i.e., the kernels attain negligible values for $\tau > \mu$).

Similar expressions result from the Wiener model of Eq. 2, where the Wiener functionals take the form of multidimensional Hermite functions in terms of the $\{v_j\}$ variables. The unknown expansion coefficients can be subsequently estimated by a least-squares fitting using the known signals (or discretized data) $y(t)$ and $\{v_j(t)\}$.

The technique has been tested thoroughly with computer simulations and yields accurate kernel estimates under the constraints discussed above. Its application to actual renal data is presented in the following section.

## RESULTS

The main result of this study is that the use of a 3rd-order Volterra-Wiener model can describe rather accurately the nonlinear pressure-flow dynamic relation in renal autoregulation. Although Volterra-Wiener applications to date have been largely limited to 2nd-order models, we were forced to extend our analysis to 3rd-order because the 2nd-order model appeared unable to explain certain significant features in the relation between the pressure and the flow signal, as demonstrated below. The extension to 3rd-order models was made possible by the Laguerre-expansion technique (LET) for three important practical reasons: (a) the compactness of kernel representation by Laguerre expansions reduced the total number of unknowns to be estimated; (b) accurate estimates can be obtained from relatively short data-records (less than 5 min experimentation time) within which the preparation may remain fairly stable; and (c) the method allows kernel estimation for experimental broadband stimuli that deviate from the requirements of strict whiteness (an inevitable experimental reality in this application).

As discussed in the Experimental Procedures and Data Collection section, experimental data from four different preparations (rats) using three different levels of broadband pressure forcing (high, medium, and low) were analyzed. Table 1 shows the mean and RMS (standard deviation) values of each data set. Pressure-flow data-records of 512 samples each (sampled at 0.5 s, for a record length of 256 s) were processed using LET to obtain 1st-, 2nd-, and 3rd-order kernels. Kernel estimation was performed by LET using the following parameters: number of kernel lags M = 60 (corresponding to memory extent of 30 s) and number of discrete-time Laguerre functions L = 8 (resulting in a total of 165 distinct expansion coefficients for the 3rd-order model). The model predictions

were computed and compared to the actual data in each case. The 3rd-order models were able to reproduce (predict) the actual flow data for the corresponding pressure data with remarkable accuracy in all cases. Table 2 summarizes the average (over the four preparations) normalized mean-square errors (NMSE) of the model predictions for each level of pressure forcing (low, medium, high) and for each model order (1st, 2nd, 3rd). Note that the 1st-order model involves only the 1st-order kernel, the 2nd-order model involves the 1st- and 2nd-order kernels, and the 3rd-order model involves the 1st-, 2nd-, and 3rd-order kernels. These results clearly demonstrate the significance of the 3rd-order kernel in representing the nonlinear pressure-flow dynamics. Note that the NMSEs also decrease with increasing power level of pressure forcing.

To further illustrate the significance of the 3rd-order kernel in renal autoregulation, we show in Fig. 1 a typical blood pressure signal (trace 1), the corresponding blood flow signal (trace 2) for an experimental run at medium power level, along with the 1st-order (trace 3), 2nd-order (trace 4), and 3rd-order (trace 5) residuals (i.e.,

**TABLE 2. Average normalized mean-square errors (NMSE) of 1st-, 2nd-, and 3rd-order Wiener model predictions for four experimental preparations.**

| | Model Order | | |
|---|---|---|---|
| Power Level | 1st-Order | 2nd-Order | 3rd-Order |
| High | 6.86% | 6.67% | 1.51% |
| Medium | 15.04% | 14.70% | 4.17% |
| Low | 18.70% | 18.63% | 7.20% |

The NMSE decreases with increasing power level and model order.

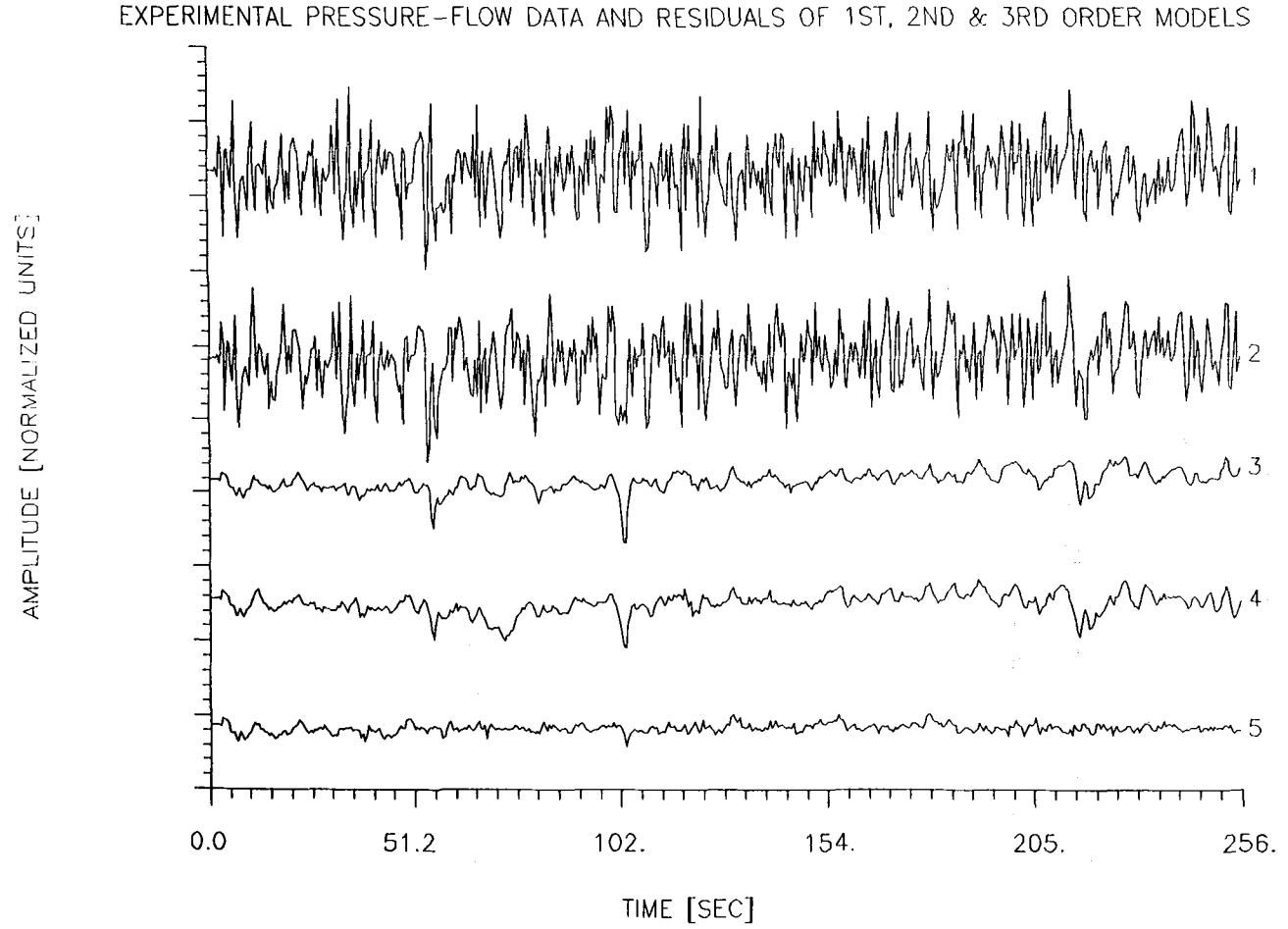


**FIGURE 1. Typical arterial blood pressure signal at the medium power level (trace 1), the associated blood flow signal (trace 2), the 1st-order residuals (trace 3), the 2nd-order residuals (trace 4), and the 3rd-order residuals (trace 5) based on Volterra-Wiener models. Note the broad band nature of these experimental pressure-flow signals, and the absence in the 3rd-order residuals of the "flow depressions" seen in the 1st- and 2nd-order residuals. The amplitude units for the pressure-flow signals are normalized to unit variance (see the Experimental Procedures and Data Collection section).**

prediction errors) based on Volterra-Wiener models of the respective order. We observe that the 1st-order model explains much of the flow signal (NMSE = 11.64%) but leaves certain significant "flow depressions" (e.g., around t = 55, 102, and 215 s in the 1st-order residuals) unexplained. The 2nd-order model slightly improves the prediction (NMSE = 10.96%) but does not remove the aforementioned "flow depressions" that are still evident in the 2nd-order residuals. However the 3rd-order model seems to capture these "flow depressions" and removes them from the 3rd-order residuals. This suggests that a significant 3rd-order nonlinearity is involved in the autoregulation process, and it can account for almost all nonlinear dynamics in this application. Note that the amplitude of the pressure-flow signals has been normalized to unit variance (see the Experimental Procedures and Data Collection section) and, therefore, the units are arbitrary. The actual physical units can be obtained by multiplying the normalized amplitude by the corresponding RMS values given in Table 1.

The same point is illustrated in the frequency domain by showing in Fig. 2 the spectrum of the actual normalized flow data (solid line) and the spectra of the 1st-, 2nd-, and 3rd-order model predictions, plotted with dotted, dashed, and dot-dashed lines, respectively. It is evident from Fig. 2 that the 3rd-order nonlinearity makes a significant contribution to the flow spectrum below 0.3 Hz. This is further illustrated in Fig. 3, where the spectra of the residuals are shown along with the flow spectrum. The inadequacy of the 1st-order (linear) and 2nd-order models below 0.3 Hz is evident by the high power spectral density of the respective residuals, especially below 0.12 Hz.

Similar results were obtained in all experiments, with certain variability observed among different preparations, as expected. For instance, the average spectra of the flow data and the model predictions for 1st-order (dotted line),

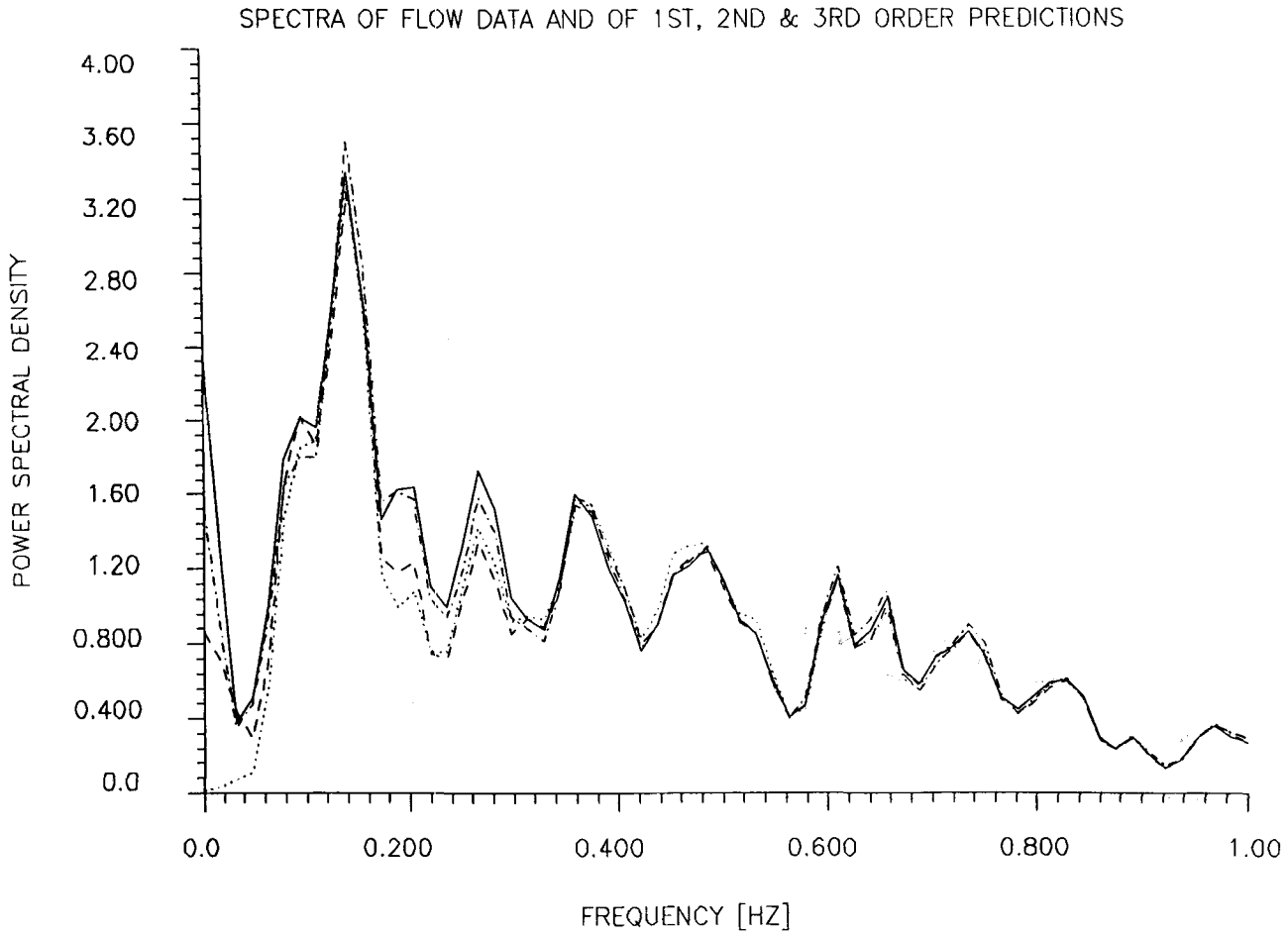


**FIGURE 2. Comparison of power spectral densities (PSD) of the normalized blood flow data of Fig. 1 (solid line) and the 1st-order (dotted line), 2nd-order (dashed line), and 3rd order (dot-dashed line) model predictions. Note the increased PSD of blood flow at frequencies below 0.03 Hz and over the resonant region 0.1–0.2 Hz. The 1st- and 2nd-order model predicted blood flow spectra exhibit greater deviations at frequencies below 0.03 Hz than does the 3rd-order model predicted blood flow spectrum.**

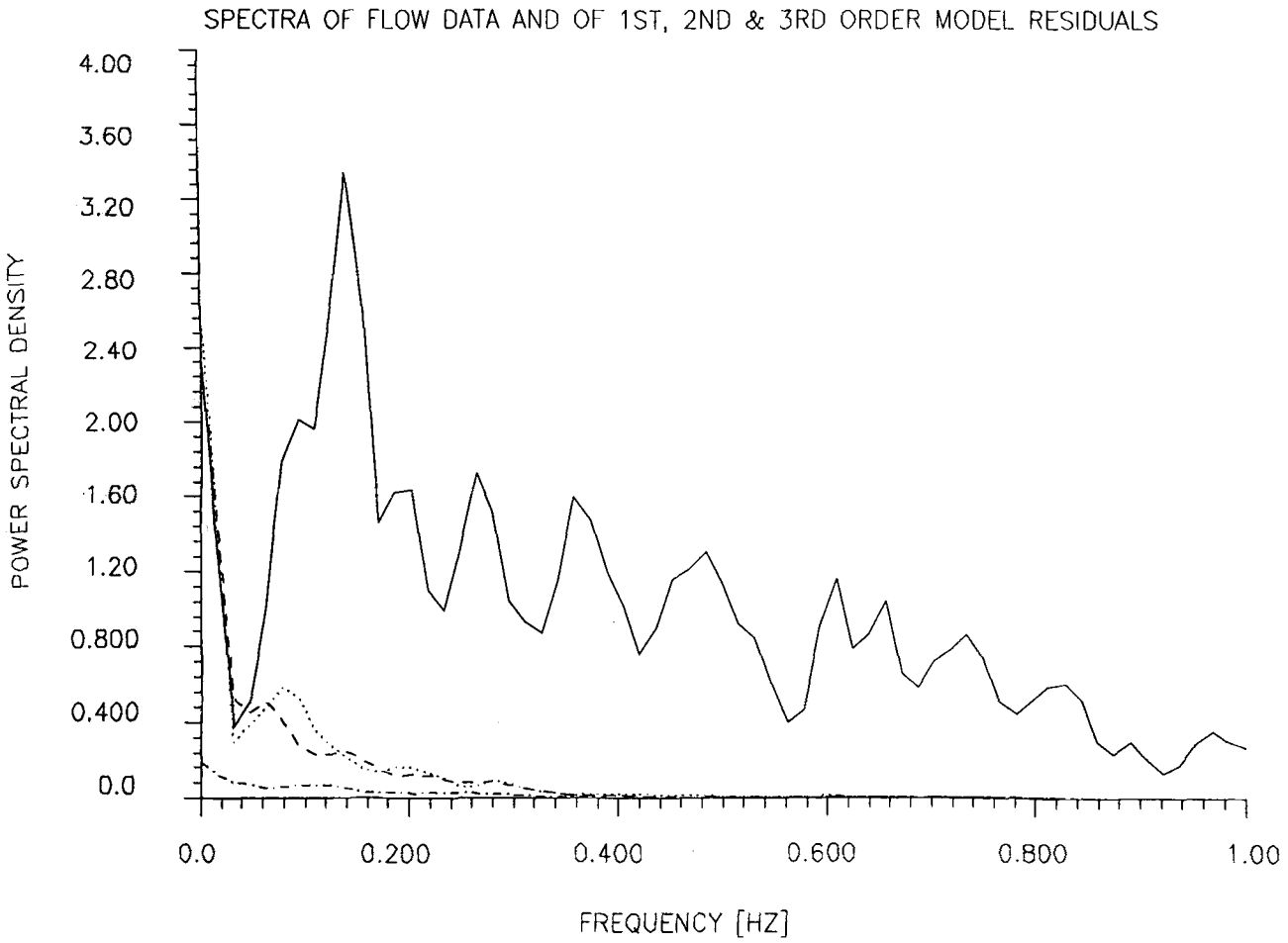


**FIGURE 3. Comparison of power spectral densities of the normalized experimental blood flow data of Fig. 3 (solid line) with the 1st-order (dotted line), 2nd-order (dashed line), and 3rd-order (dot-dashed line) residual spectra. Note the significant residual power spectral density at frequencies below 0.3 Hz for both the 1st- and 2nd-order model residuals.**

2nd-order (dashed line), and 3rd-order (dot-dashed line) are shown in Fig. 4 for the medium level group. Likewise the average spectra of the residuals and flow data for medium level are shown in Fig. 5.

Note that the aforementioned "flow depressions" in the 1st-order residuals are more pronounced for medium and low level of forcing, and the degree of 3rd-order nonlinearity (as measured by the percentage contribution of the 3rd-order kernel) follows the same pattern, as shown in Table 2. This suggests that the presence of nonlinear autoregulation is least evident at the high level of forcing, leading us to suggest that the TGF may become "overwhelmed" at high levels of pressure forcing.

Turning to the obtained 1st-order kernel estimates, we note that they vary slightly for different preparations at the same forcing level, but exhibit significant changes of waveforms for different levels of forcing. For instance, Fig. 6 shows the 1st-order kernel estimates for low (solid), medium (dotted), and high (dashed) levels of forcing for a single preparation (rat). Note that the amplitude units are arbitrary, since the pressure/flow data have been normalized (see figure caption). We observe that these waveforms become more damped as the level of forcing increases. This is suggestive of nonlinear feedback, based on previously reported analysis and simulation results of a class of nonlinear feedback systems (11). The changes observed experimentally in the 1st-order kernel estimates may be explained, in general, by a system of this class with negative compressive (sigmoid type) feedback. In order to test this hypothesis, a necessary (but not sufficient) condition is that the differences between these kernels exhibit the same waveform (11). Indeed, the computed differences of the low and medium level kernels from the high level kernel are shown in Fig. 7 and appear to have rather similar waveforms. This observation suggests that the mechanisms of renal autoregulation may employ negative compressive (e.g., sigmoid type) feedback.

The average 2nd-order kernel estimates are shown in

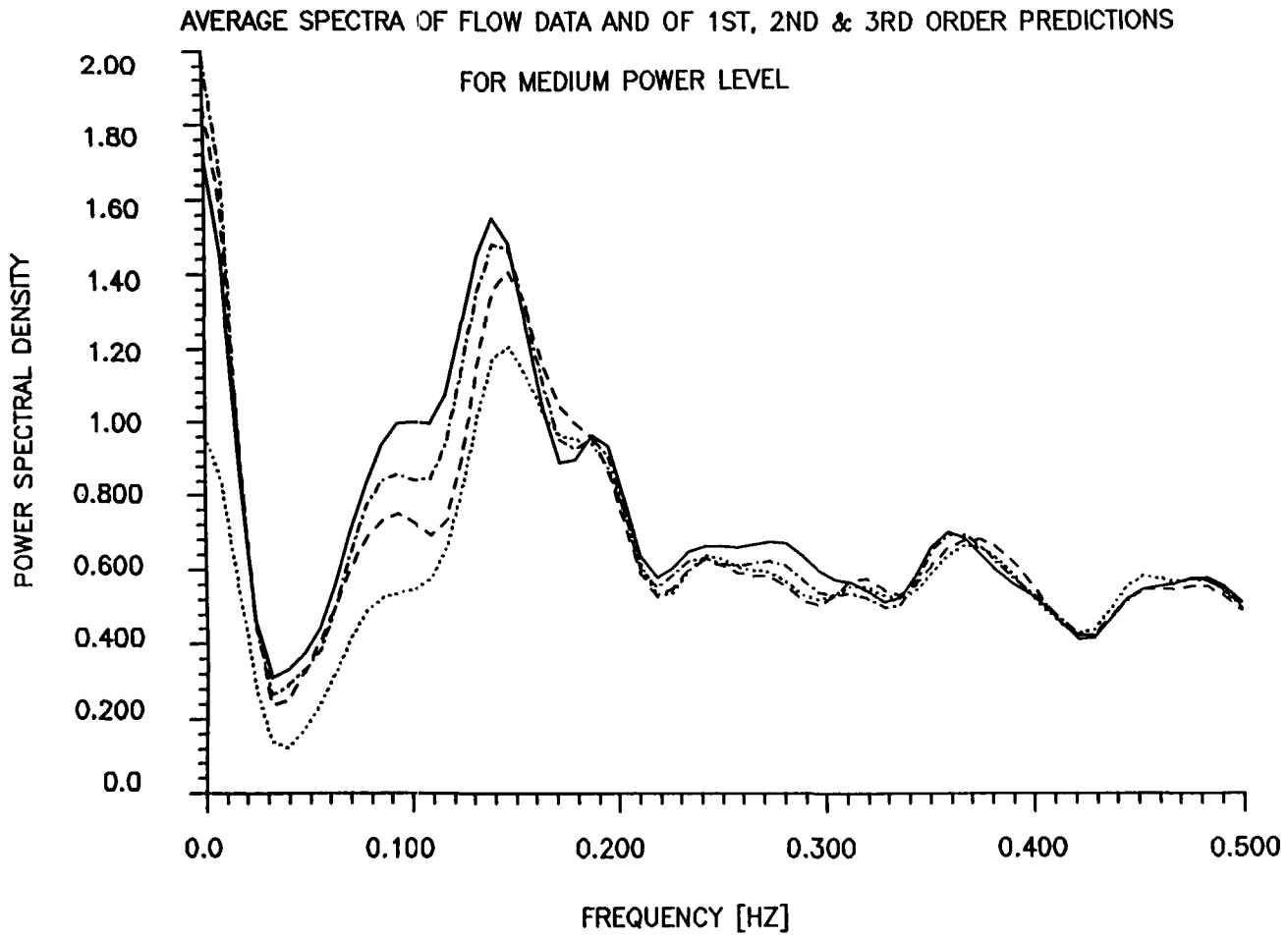


**FIGURE 4. Comparison of average power spectral densities of the normalized experimental blood flow (solid line), 1st-order (dotted line), 2nd-order (dashed line), and 3rd-order (dot-dashed line) model predictions at the medium power level forcing. Significant improvement is observed in the 3rd-order model predicted spectrum at frequencies below 0.2 Hz.**

Fig. 8 for high, medium, and low level of forcing, respectively. They exhibit distinct shapes, indicative of the complexity of the underlying nonlinear feedback configuration. Their amplitude is about one order of magnitude smaller than their 1st-order counterparts. Note that we can draw inferences regarding the relative significance of the 1st-order and 2nd-order kernels by comparing their respective amplitudes, because the pressure/flow (input/output) data have been normalized to unit variance. Thus, the shown amplitude units are not physical but allow such comparisons of relative significance.

The same comments apply to the obtained 3rd-order kernel estimates, for which we show the average 3-D cut at $\tau_3 = 0$ in Fig. 9 for high, medium, and low level of forcing, respectively. The high dimensionality (4-D) of the 3rd-order kernel points to the desirability of reducing the 3rd-order model to a more compact block-structured model, involving linear and static nonlinear components. We note that the 3rd-order (as well as the 2nd-order) kernel estimates vary significantly in shape for different forcing levels (i.e., variance of pressure fluctuations), as well as for different mean values of applied pressure (which essentially determine the "operating points" on the nonlinear feedback curves). This suggests that precise analysis of these high-order kernels be based on measurements obtained from a single preparation (rat) and for distinct pressure forcings (i.e., averaging will probably obscure the detailed analysis of these waveforms as they change for different forcing levels).

## CONCLUSIONS AND DISCUSSION

All previous studies of the dynamic characteristics of renal autoregulation of blood flow have used linear systems analysis (1,2,4,15). The methods employed have been

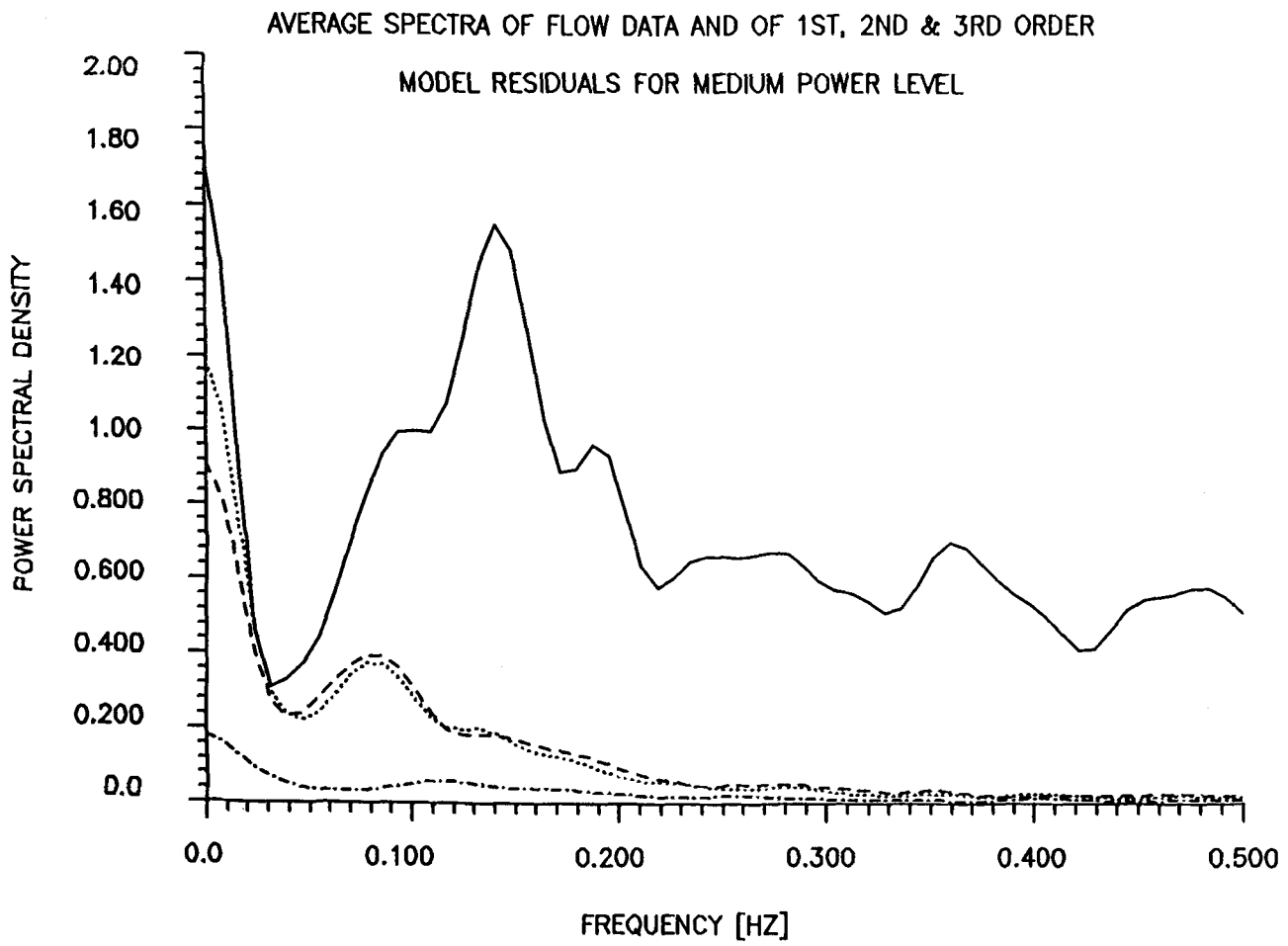


**FIGURE 5. Comparison of average power spectral densities of the normalized experimental blood flow (solid line) with 1st-order (dotted line), 2nd-order (dashed line), and 3rd-order (dot-dashed line) model residuals for the medium power level forcing. The inadequacies of 1st- and 2nd-order models are especially evident at frequencies below 0.1 Hz.**

either cross-spectral methods using the Fast Fourier Transform (2,4,15), or have employed autoregressive-moving average (ARMA) models to characterize the transfer function for renal autoregulation (1). Calculations of the coherence function (4), and/or the residual spectrum for the models (1), have clearly shown the presence of significant nonlinearities in the frequency range below 0.1–0.12 Hz. This is especially important since it is in this frequency range where the autoregulatory mechanisms are active in minimizing perturbations in renal function caused by fluctuations in the arterial pressure. The sole reliance on linear methods may have caused significant bias in the determination of the transfer function for the system, and development of appropriate methods to characterize the nonlinear properties of the autoregulatory system is therefore highly warranted.

The present study shows that practicable estimation of 3rd-order Volterra-Wiener models from short experimental records is possible with a kernel estimation technique using Laguerre expansions (12). These 3rd-order models account for almost all nonlinear dynamic relationships in the experimental broadband pressure-flow data. In particular, it has been shown that the 3rd-order kernel plays an important role in explaining sudden "depressions" in renal blood flow (possibly due to the TGF mechanism) in response to broadband arterial blood pressure forcing. This is probably due to the fact that the sigmoid-type nonlinearity (with the two-sided limiting characteristics observed previously in TGF) requires at least a 3rd-order term to approximate it (i.e., a 1st-order, and 2nd-order term will not approximate the essential characteristics of a sigmoid nonlinearity). These "flow depressions" could not be explained in the past using linear analysis methods, and they are responsible, at least in part, for the failure of previous linear models in the frequency range below 0.12 Hz.

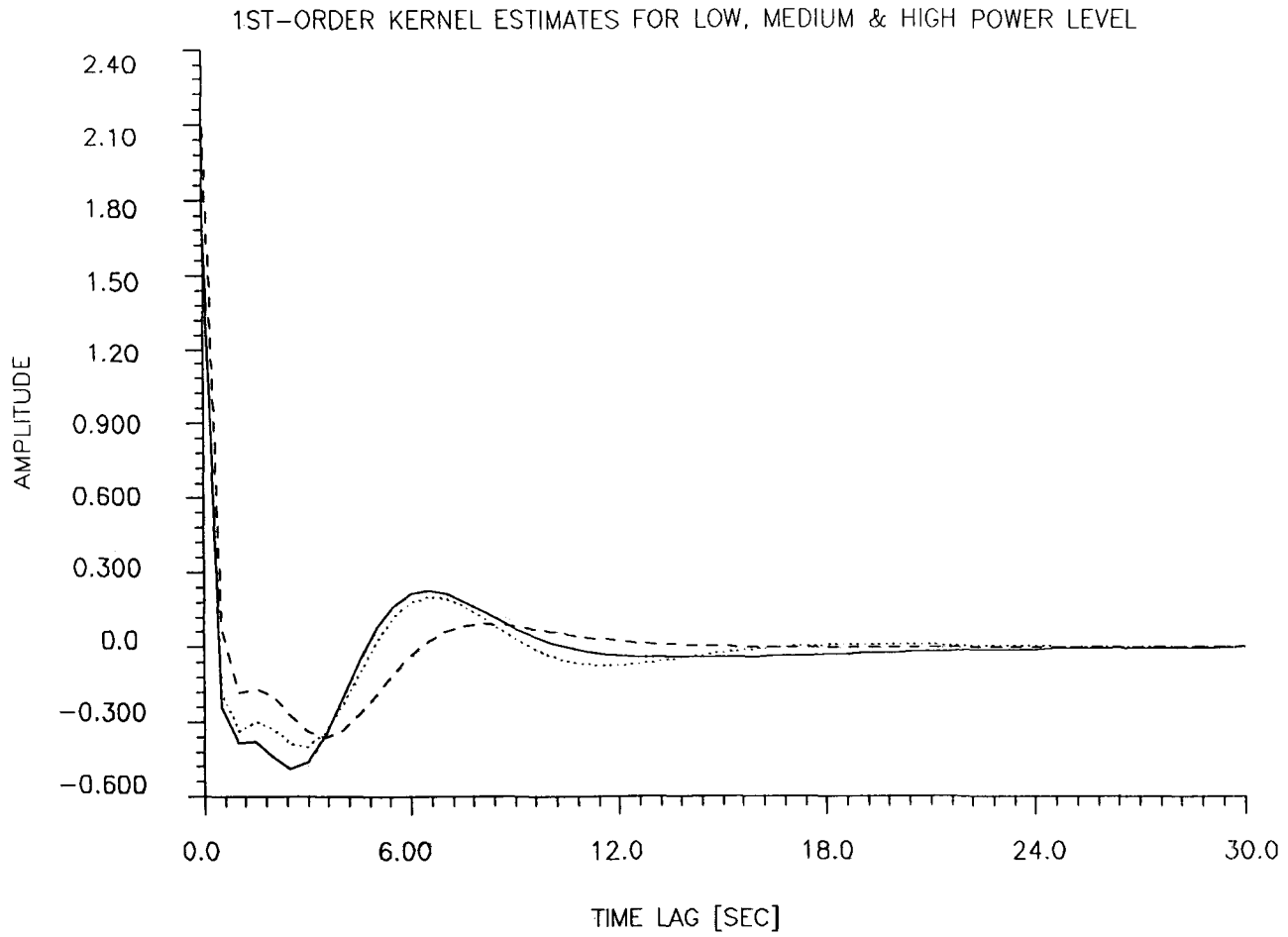


**FIGURE 6. Typical 1st-order kernel estimates at the high (dashed line), medium (dotted line), and low (solid line) power levels of arterial pressure forcings, obtained from the same preparation (rat). Note the increased damping of the waveforms as the level of arterial pressure forcing increases. The amplitude units of these kernels are arbitrary, since the pressure-flow data were normalized to unit variance. In general, the 1st-kernel units are: (output units)/(input units)/(time units). Actual units can be obtained by use of the corresponding RMS values of pressure/flow (input/output) given in Table 1.**

The present measurements were by necessity conducted in anesthetized animals, and it cannot be excluded that the anesthetics may have influenced the results. However using linear analysis of broadband pressure-flow data, identical results have been obtained from experiments where the rats have been anesthetized with either the gas anesthetic halothane as in the present study, or with the thiobarbiturate inactin (2,4,15). In fact, the sudden "depressions" in renal blood flow were originally observed in inactin anesthetized rats (unpublished results). Therefore, we do not believe that the choice of anesthetic has affected the results to any major extent. It would of course be preferable to perform the experiments in conscious, unanesthetized animals, but this is not possible with the existing technology.

It is anticipated that the present method will be useful in determining the functional consequences of several nonlinear phenomena occurring at the level of the single nephron. Thus, measurements of single nephron blood flow using laser Doppler flowmetry have demonstrated the presence of two oscillatory components (21). The major oscillatory component has a frequency of 0.03–0.04 Hz and is caused by the TGF mechanism (3). Because of time lags and its nonlinear characteristics, the TGF system appears to enter into a stable oscillatory mode (3). In addition, a smaller oscillatory component with a frequency of 0.12–0.14 Hz can be also found in the single nephron blood flow (21). The origin of this component is presently unknown. An important question is what physiological role these self-sustained oscillations at the single nephron level play in the overall regulation of renal hemodynamics. Because of the inherent nonlinear properties of

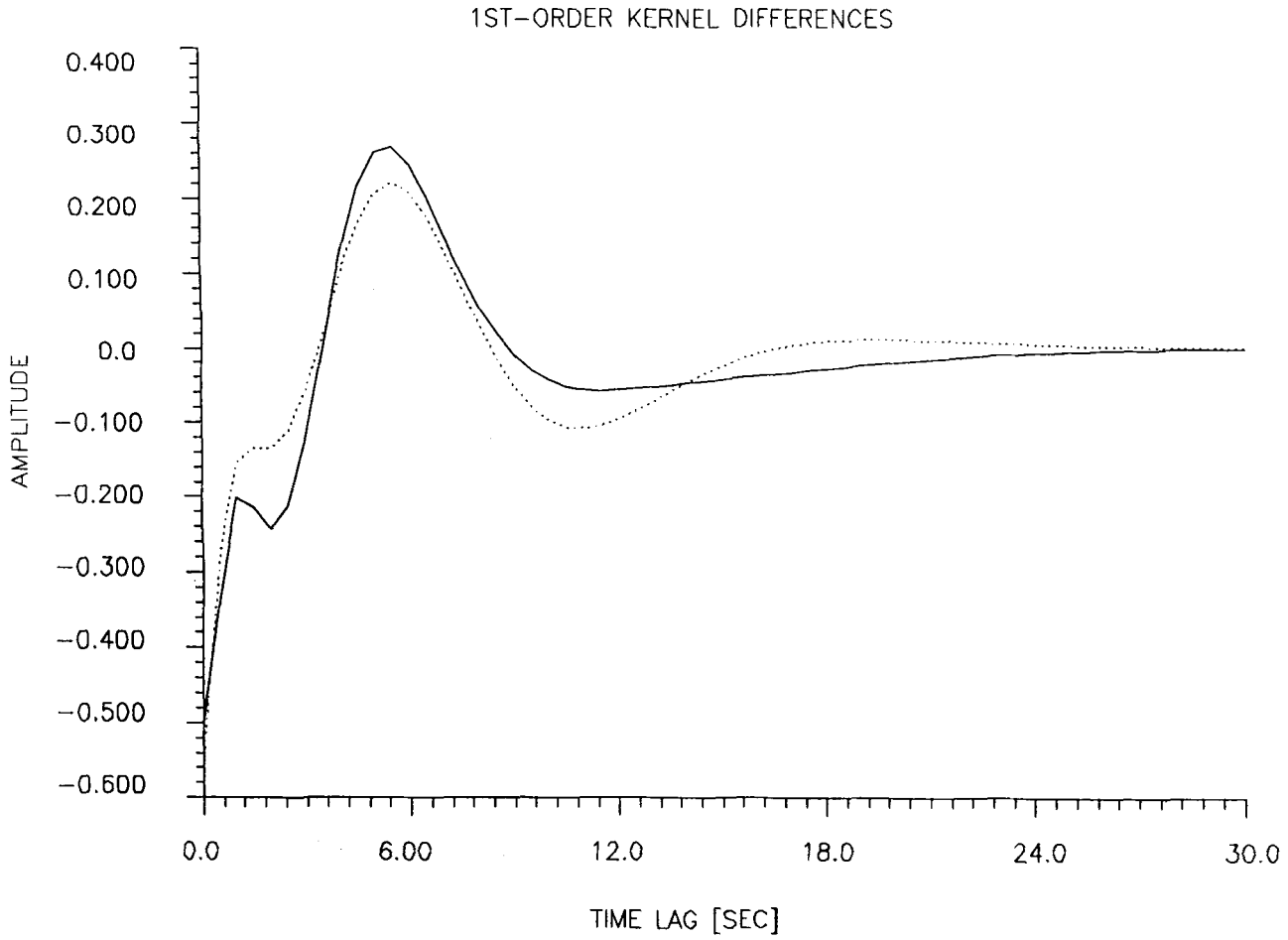


**FIGURE 7. The 1st-order kernel differences obtained by subtracting the high power level kernel from the low power level kernel (solid line) and the medium power level kernel (dotted line). Note the similarity in these 1st-order kernel differences, which suggests the presence of nonlinear feedback.**

self-sustained oscillators, such studies will require the use of nonlinear methods.

In spontaneously hypertensive rats (SHR), the regular oscillations observed in the various variables at the single nephron level are replaced by irregular fluctuations (20). Most likely, this is due to a transition of the TGF system to a dynamic range dominated by chaotic dynamics (21). Again, the functional consequences of this change at the organ level are not known, and the elucidation of this question will undoubtedly require the use of nonlinear methods for systems analysis.

In the present study the waveform of the 1st-order kernel varied with the power level of the forcing. The changes observed are suggestive of nonlinear negative compressive (sigmoid type) feedback in the renal autoregulatory mechanisms. This inference is based on previously published analysis and simulations of a class of nonlinear feedback systems (11). The precise determination of the underlying feedback configuration (probably composed of two loops corresponding to the two autoregulatory mechanisms) and the identification of the functional characteristics of the various feedforward and feedback components are currently under study. This is a task of considerable complexity due to the fact that several possible configurations must be explored. The identification of the various components of this nonlinear feedback configuration may lead to an equivalent (and more compact) block-structured model.

The present results are a first glance at the nonlinear dynamics of renal autoregulation (with the detail and quantification afforded by the Volterra-Wiener approach) and they are far from the final word on this subject. Future work will apply these methods to study the implications of the nonlinearities at the single nephron level for the regulation of overall renal hemodynamics. In addition, future work must address the important issue of con-

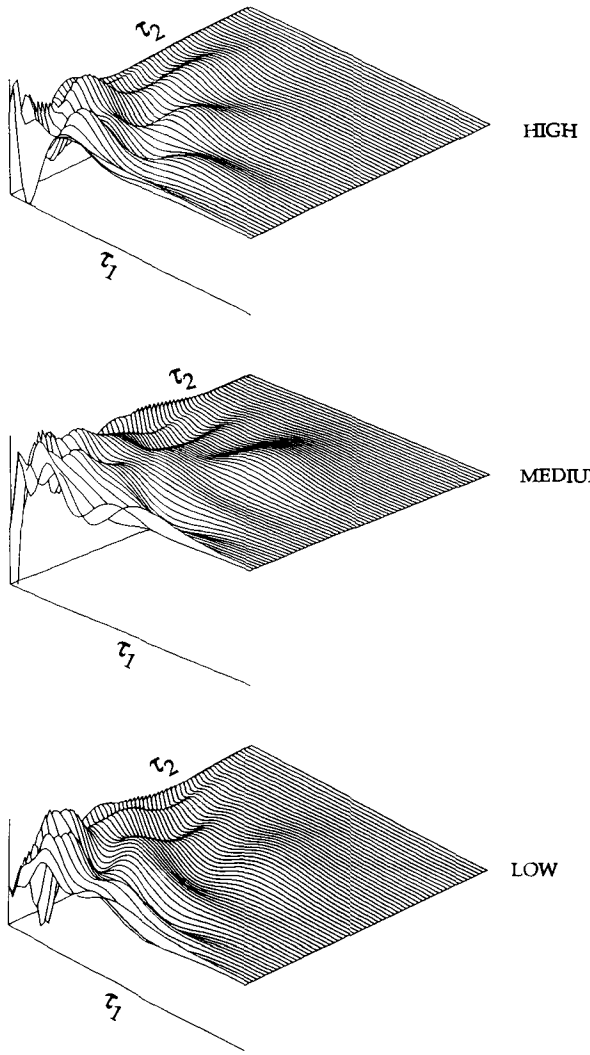


FIGURE 8. The average 2nd-order kernel estimates for the high, medium, and low power level forcings. The minimum and maximum amplitudes of the 2nd-order kernels are (−0.044 and 0.022) for high, (−0.088 and 0.025) for medium, and (−0.053 and 0.032) for low power level forcings. The amplitude units are arbitrary since the pressure/flow data were normalized. In general, the 2nd-order kernel units are: (output units)/(input units)$^2$/(time units)$^2$. The two time-lag axes ($\tau_1$,$\tau_2$) range from 0 to 30 seconds.

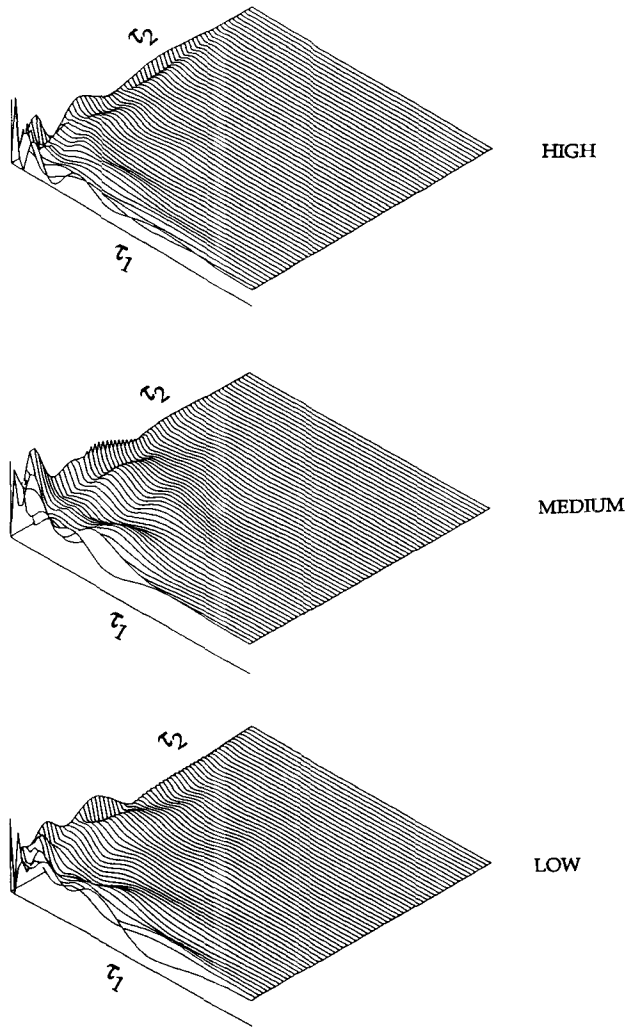


FIGURE 9. The average 3rd-order kernel estimates (3D-cut at $\tau_3 = 0$) for the high, medium, and low power level forcings. The minimum and maximum amplitudes of the 3rd-order kernels are (−0.01 and 0.03) for high, (−0.015 and 0.024) for medium, and (−0.027 and 0.047) for low power level forcings. The amplitude units are arbitrary since the pressure/flow data were normalized. In general, the 3rd-order kernel units are: (output units)/(input units)$^3$/(time units)$^3$. The two time-lag axes ($\tau_1$,$\tau_2$) range from 0 to 30 seconds.

verting the high-order kernel characterizations of the autoregulatory process into an understandable compact block-structured model. This is expected to facilitate the physiological interpretation of the modeling results.

## REFERENCES

1. Chon, K.H.; Chen, Y.M.; Holstein-Rathlou, N.-H.; Marsh, D.J.; Marmarelis, V.Z. On the efficacy of linear system analysis of renal autoregulation in rats. IEEE Trans. Biomed. Eng. BME 40:8-20; 1993.
2. Daniels, F.H.; Arendshorst, W.J.; Roberds, R.G. Tubuloglomerular feedback and autoregulation in spontaneously hypertensive rats. Am. J. Physiol. (Renal Fluid Electrolyte Physiol. 27) 258:F1479-F1489; 1990.
3. Holstein-Rathlou, N.-H.; Marsh, D.J. A dynamical model of the tubuloglomerular feedback mechanism. Am. J. Physiol. (Renal Fluid Electrolyte Physiol. 27) 258:F1448-F1459; 1990.
4. Holstein-Rathlou, N.-H.; Wagner, A.J.; Marsh, D.J. Tubuloglomerular feedback dynamics and renal blood flow autoregulation in rats. Am. J. Physiol. (Renal Fluid Electrolyte Physiol. 29) 260:F53-F68; 1991.
5. Korenberg, M.J. Functional expansions, parallel cascades and nonlinear difference equations. In: Marmarelis, V.Z.,

ed. Advanced methods of physiological system modeling: Vol. I. Los Angeles: Biomedical Simulations Resource, University of Southern California; 1987: pp. 221–240.
6. Lee, Y.W.; Schetzen, M. Measurement of the Wiener kernels of a nonlinear system by cross-correlation. Int. J. Control 2:237–254; 1965.
7. Marmarelis, P.Z.; Marmarelis, V.Z. Analysis of physiological systems: The white noise approach. New York: Plenum; 1978.
8. Marmarelis, V.Z. A family of quasi-white random signals and its optimal use in biological system identification. Part I: Theory. Biol. Cyb. 27:49–56; 1977.
9. Marmarelis, V.Z., ed. Advanced methods of physiological system modeling: Vol. I. Los Angeles: Biomedical Simulations Resource, University of Southern California; 1987.
10. Marmarelis, V.Z., ed. Advanced methods of physiological system modeling: Vol. II. New York: Plenum; 1989.
11. Marmarelis, V.Z. Wiener analysis of nonlinear feedback in sensory systems. Ann. Biomed. Eng. 19:345–382; 1991.
12. Marmarelis, V.Z. Identification of nonlinear biological systems using Laguerre expansions of kernels. Ann. Biomed. Eng. 21:573–589; 1993.
13. Marsh, D.J.; Osborne, J.L.; Cowley, A.W. 1/f fluctuations in arterial pressure and the regulation of renal blood flow in dogs. Am. J. Physiol. (Renal Fluid Electrolyte Physiol. 27) 258:F1394–F1400; 1990.
14. Rugh, W.M. Nonlinear system theory: The Volterra/Wiener approach. Baltimore: Johns Hopkins University Press; 1981.
15. Sakai, T.; Hallman, E.; Marsh, D.J. Frequency domain analysis of renal autoregulation in the rat. Am. J. Physiol. (Renal Fluid Electrolyte Physiol. 19) 250:F364–F373; 1986.
16. Schetzen, M. The Volterra and Wiener theories of nonlinear systems. New York: Wiley; 1980.
17. Schnermann, J.; Briggs, J.P. Function of the juxtaglomerular apparatus: Control of glomerular hemodynamics and renin secretion. In: Seldin, D.W.; Giebisch, G. The kidney: Physiology and pathophysiology. 2nd ed. New York: Raven Press; 1992: pp. 1249–1289.
18. Watanabe, A.; Stark, L. Kernel method for nonlinear analysis: Identification of a biological control system. Math. Biosci. 27:99–108; 1975.
19. Wiener, N. Nonlinear problems in random theory. New York: Wiley; 1958.
20. Yip, K.P.; Holstein-Rathlou, N.-H.; Marsh, D.J. Chaos in blood flow control in genetic and renovascular hypertensive rats. Am. J. Physiol. (Renal Fluid Electrolyte Physiol. 30) 261:F400–F408; 1991.
21. Yip, K.P.; Holstein-Rathlou, N.-H.; Marsh, D.J. Mechanisms of temporal variations in single nephron blood flow in the rat. Am. J. Physiol. (in press).